New scaling relations from CESAM and MESA models for mass and radius of post-MS stars: application to Kepler Legacy stars

T. Çakır Alsaç,[1,2]★ † M. Yıldız,[2] ‡, Sibel Örtel[1,2] §
[1]Ege Üniversitesi, Fen Bilimleri Enstitüsü, Bornova, 35100, İzmir, Türkiye
[2]Ege Üniversitesi, Astronomi ve Uzay Bilimleri Bölümü, Bornova, 35100, İzmir, Türkiye

Accepted XXX. Received YYY; in original form ZZZ

ABSTRACT

The precise determination of the fundamental parameters of stars is crucial for understanding stellar structure and evolution. In this regard, the asteroseismic parameters of solar-like oscillating stars obtained from space telescopes are very useful for determining the mass (M) and radius (R) of single stars using classical scaling relations. These relations still need to be improved. Alternative scaling relations based on the reference frequencies ($\nu_{\rm min}$) due to the helium ionization zone glitches are developed for the main-sequence (MS) stars and applied to Kepler Legacy (KL) stars by Yıldız, Çelik Orhan, & Kayhan (2019). In this study, MS and post-MS CESAM and MESA models are compiled from the literature, and new scaling relations are developed for R and gravity of evolved stars for the first time. The expressions for R and gravity are simultaneously derived as functions of the large frequency separation, $\nu_{\rm min}$, and metallicity. New scaling relations for radius and gravity are derived using two different methods: quadratic and logarithmic. We also investigate whether the derived relations depend on the choice of stellar evolution model, and find that both codes yield consistent results, suggesting that the relations are model-independent. These derived relations based on $\nu_{\rm min1}$ are applied to a sample of 31 KL sub-giant stars with masses ranging from 0.85–1.74 $M_\odot$ and radii ranging from 1.03–2.82 $R_\odot$. Furthermore, using simultaneous solutions, we estimate new mass and radius ranges of 0.89–1.62 $M_\odot$ and 1.04–2.95 $R_\odot$, respectively. The results demonstrate significant improvements in the determination of M and R for evolved KL stars, highlighting the potential of the new scaling relations in asteroseismic analyses.

Key words:
stars: asteroseismology, stars: evolution, stars: reference frequencies, stars: fundamental parameters, stars: solar-type, stars: oscillations.

1 INTRODUCTION

Stars are celestial bodies that generate energy through nuclear reactions in their cores, transport this energy from the interior to the surface, and radiate it into space. Understanding the interior structure and evolution of these objects is one of the main goals of astrophysics. Therefore, it is very important to determine the fundamental parameters of the star: mass (M), radius (R), luminosity (L), age (t), helium abundance (Y), and heavy element abundance (Z). Asteroseismology provides comprehensive information about the deep stellar interior (Aerts 2021). One of its main purposes is to determine the fundamental parameters of stars using the oscillation frequencies of stars. In this direction, CoRoT (Baglin et al. 2006), Kepler (Borucki et al. 2010), and TESS (Ricker et al. 2015) space telescopes were launched with the expectation that many planets, in particular Earth-sized and smaller planets in the habitable zone of other stars, would be discovered. These space missions have greatly contributed to the development of asteroseismology. High-quality photometric data have been obtained with more precise and comprehensive measurements. Kepler's success with its accuracy in seismic data is still at the forefront.

The M and R of oscillating stars can be found from the classical scaling relations using the frequency of maximum amplitude ($\nu_{\rm max}$) determined from asteroseismic data, mean value of the large separation between oscillation frequencies ($\Delta\nu$) and the effective temperature ($T_{\rm eff}$). The development of asteroseismology provides very important information about the interior structure and evolution of solar-like oscillating stars. Reference frequencies ($\nu_{\rm min}$) are another set of parameters that play an important role in determining the fundamental stellar properties (Yıldız et al. 2014). The detected oscillation frequencies are spaced very regularly in these stars. The glitches caused by the He II ionization zone constitute the reference frequencies. Yıldız, Çelik Orhan, & Kayhan (2019) used these reference frequencies in scaling relations to determine the fundamental properties ($T_{\rm eff}$, M and R) of main sequence (MS) stars. The use of new scaling relations based on reference frequencies has led to significant improvements over classical scaling relations. In this study, we develop similar new asteroseismic methods and apply them to subgiant stars observed by Kepler. The reliability of such methods

★ E-mail: tubanurcakir97@gmail.com
† ORCID: 0000-0002-2538-0105
‡ ORCID: 0000-0002-7772-7641
§ ORCID: 0000-0001-5759-7790

depends on the accurate and precise determination of the asteroseismic parameters used.

Asteroseismic methods are powerful tools that provide direct insights into the interior structure of stars. To interpret oscillation frequencies correctly and to derive reliable asteroseismic parameters (e.g., $\Delta\nu$ and ν_{max}), accurate knowledge of stellar mass and metallicity is essential. These parameters are closely related to a star's mean density, surface gravity, and interior profiles, all of which depend on mass and Z. Accurate determination of these quantities is therefore necessary to meaningfully interpret results obtained from both classical and asteroseismic analyses.

In this study, we develop new scaling relations for stellar M and R, as the classical relations (e.g., see Chaplin et al. 2011) often suffer from limited precision, particularly due to the uncertainties associated with ν_{max}. In particular, due to the large uncertainty in ν_{max}, we use reference frequencies in the relations we propose. We derive new scaling relations for radius and mass using MS and post-main sequence (post-MS) models generated with the CESAM (Marques, Monteiro, & Fernandes 2008) and MESA (Paxton et al. 2011, 2013, 2015, 2018, 2019; Jermyn et al. 2023) evolution codes. We analyze whether the scaling relations obtained from the two models are model-dependent. We formulate the new scaling relations for M and R using two different methods, and apply them to the Kepler Legacy stars (KLs). Finally, we write a Python code (version 3.13.2) [1] to compute the mass and radius of all KLs collectively.

This paper is organized as follows. In Section 2, we present the properties of the models constructed using the CESAM and MESA evolutionary codes, and compile a scaling relation for radius from the literature. In the same section, we compute the seismic parameters (ν_{max}, $\Delta\nu$, $\delta\nu_{02}$) from the oscillation frequencies of the CESAM models and describe how their reference frequency are determined. Section 3 is devoted to deriving new scaling relations for mass and radius using the new methods. In Section 4, we apply the derived relations to the Kepler legacy stars and compare the results with the seismic values reported in the literature. Finally, the conclusions of our study are presented in Section 5.

2 MODELS CONSTRUCTED BY USING THE MESA AND CESAM CODE

Interior models are derived by solving four non-linear stellar structure equations: the conservation of mass, hydrostatic equilibrium, thermal balance and temperature gradient. In this study, we derive scaling relations for radius and mass using MS and post-MS models constructed with the stellar evolution codes CESAM and MESA. These codes allow us to construct stellar models across a wide mass range from low-mass stars to massive stars, including the Sun, by varying the input parameters. Additionally, they enable estimation of the oscillation frequencies of stars that have not yet been observed. Computing grids of stellar evolution tracks allows the study of a large number of stellar types.

The scaling relations for the radius from the models are computed using the stellar evolution model grids CESAM code (Morel 1997; Morel & Lebreton 2008), version 2k. A new version of CESAM developed by Marques (2008) was used to generate grids with different initial parameters. The models extend from the main sequence of zero age (ZAMS) to the beginning of the red giant branch (RGB). They are no-diffusion models with masses ranging from 0.8 to 8 $M_\odot$ and do not take into account the overshooting of the convective core. The chemical composition (Y = 0.28 and Z/X = 0.02857) is the solar composition. In the calculations, an isothermal atmosphere was assumed at the top. OPAL tables (Rogers, Swenson, & Iglesias 1996; Iglesias & Rogers 1996; Alexander & Ferguson 1994) were used for opacity at different temperatures. Models were computed with the GN93 solar mixture of heavy elements ($(Z/X)_\odot = 0.0245$) (Grevesse & Noels 1993). Standard mixing length treatment of Böhm-Vitense (1958) and Henyey, Vardya, & Bodenheimer (1965) is assumed for the convection theory.

The Porto Oscillations Code (POSC) (Monteiro 2008) was used to compute the oscillation frequencies of models. The frequency files contain oscillation frequencies of modes in the range $0 \leq l \leq 3$. In this study, 1.0 and 1.1 $M_\odot$ models with frequency files are used. The MS radius range covered by these mass values is 0.91–1.32 $R_\odot$, while the post-MS radius range is 1.22–2.13 $R_\odot$.

In this study, some of the models used were constructed using the MESA evolution code. These models are used to derive alternative scaling relations for mass and radius. The MESA evolution code (Paxton et al. 2011, 2013) integrates many numerical and physics modules for a variety of stellar evolution scenarios, including advanced stages of star evolution from low-mass stars to massive stars. The models used in this study are taken from Kayhan, Yıldız, & Çelik Orhan (2019), which includes 20 host stars. These models cover MS mass range of 0.74–1.27 $M_\odot$ and post-MS mass range of 1.07–1.55 $M_\odot$. The corresponding radius ranges for these masses are 0.75–1.42 $R_\odot$ and 1.25–2.10 $R_\odot$, respectively. Standard mixing length theory (Böhm-Vitense 1958) was assumed for convection theory in these models. For opacity at high temperatures, OPAL (Iglesias & Rogers 1993, 1996) tables and low-temperature tables of Ferguson et al. (2005) were used. Nuclear reaction rates are computed using Angulo et al. (1999) updated by Kunz et al. (2002) and Cyburt et al. (2010). For atmospheric conditions in the host star models, the `simple_photosphere` option is selected in MESA. Diffusion models have been developed for host stars with masses $M_{star} < 1.2\ M_\odot$. Diffusion is not considered for stars larger than this mass.

The oscillation frequencies were derived using the ADIPLS package (Kjeldsen, Bedding, & Christensen-Dalsgaard 2008) within MESA. Model ν_{max} value was determined from the relation in Brown et al. (1991). Solar values ($\nu_{max\odot} = 3050\ \mu$Hz (Stix 1989) and $T_{eff\odot} = 5777$ K (Kjeldsen & Bedding 1995)) were used in the calculations. The mean values of large separation and small separation were computed from the model oscillation frequencies. The ν_{min} of the models were determined using the method described in Yıldız et al. (2014).

2.1 Scaling relation for radius

Scaling relations are important for determining the fundamental parameters of stars by seismic methods. For this, we need some seismic parameters. In solar-like oscillating stars, the He II ionization zone causes small glitches at regular intervals and allows the formation of reference frequencies.Yıldız, Çelik Orhan, & Kayhan (2019) used these frequencies, in addition to the ν_{max} and $\Delta\nu$ parameters used in classical scaling relations. They computed the masses, radii, and ages of 90 stars by deriving new scaling relations, including relations based on ν_{min}. The radii of these stars computed from ν_{min0} and ν_{min1} are very close and the differences between less than 0.007 $R_\odot$. The scaling relations obtained for mass and radius are derived from MS models and applied to Kepler legacy stars. It is found that these scaling relations show a slight dependence on the metallicity. Therefore, a new method was developed to compute the initial metallicity

[1] Python Software Foundation. Python Language Reference, version 3.13.2. Available at: https://www.python.org

(Z_0) from the surface metallicity (Z_s), taking into account the effect of microscopic diffusion. The scaling relation for the radius based on $\nu_{\rm min1}$ ($R_{\rm sis1}$) from the MS models (Yıldız, Çelik Orhan, & Kayhan 2019):

$$R_{\rm sis1}/R_{\odot} = \frac{\left(\frac{\nu_{\rm min1}}{\nu_{\rm min1\odot}}\right)^{0.156}\left(\frac{\Delta\nu_{\odot}}{\Delta\nu}\right)^{0.92}}{\left(1.14\,(r_{T\Gamma}-1.11)^2+0.98\right)(-0.64 r_{\delta\Delta}+1.05)}. \quad (1)$$

Here, the denominator includes terms involving the adiabatic exponent (Γ_1) and small frequency separation ($\delta\nu_{02}$). Since Γ_1 and $\delta\nu_{02}$ are not available in CESAM models, we use only the leading term. Thus, $R_{\rm sis1}$ becomes as follows:

$$\frac{R_{\rm sis1}}{R_{\odot}} \approx \left(\frac{\nu_{\rm min1}}{\nu_{\rm min1\odot}}\right)^{0.156}\left(\frac{\Delta\nu_{\odot}}{\Delta\nu}\right)^{0.92}. \quad (2)$$

By expressing $\nu_{\rm min1}$ in function of $\nu_{\rm min0}$ ($\nu_{\rm min1} \propto \nu_{\rm min0}^{1.042}$), they obtain an equation similar to the one derived for $R_{\rm sis1}$ for $R_{\rm sis0}$. We derive the R-$\nu_{\rm min}$ relation for post-MS for the first time in this study. First of all, we must determine the reference frequency in equation (2) to obtain the radius from the seismic way. To this end, we plotted $\Delta\nu$–ν graphs based on CESAM MS and post-MS models using Gnuplot version 5.4 [2]. We identified the minima in a specific frequency range. To determine the frequency corresponding to a specific minimum, it is sufficient to derive the linear equations that describe the slopes on either side of the dip. The point where these two lines intersect gives the frequency of $\nu_{\rm min1}$. In general, $\nu_{\rm min1}$ is much deeper than $\nu_{\rm min0}$. This allows a better determination of $\nu_{\rm min1}$ among the reference frequencies. Therefore, it is expected that the radii computed with $\nu_{\rm min1}$ will give more accurate results. We determine $\nu_{\rm min0}$, $\nu_{\rm min1}$ and $\nu_{\rm min2}$ from the oscillation frequencies of the models using this method. The model data together with other determined seismic parameters are listed in Tables 1 and 2. The uncertainty in the reference frequencies, especially for $\nu_{\rm min1}$ and $\nu_{\rm min2}$, is very small compared to $\Delta\nu$ in most cases, about one tenth of $\Delta\nu$.

Most stars have many minima in both their observation and model oscillation frequencies. The numbering of these minima is very important. The reference frequencies we obtained are plotted versus $\nu_{\rm max}$ in Fig. 1. For comparison purposes, the reference frequencies obtained in the study by Yıldız, Çelik Orhan, & Kayhan (2016) are also provided. We determine that the reference frequencies of the 1.0 and 1.1 $M_{\odot}$ post-MS models are consistent with the MESA model results. These reference frequencies, along with the $\Delta\nu$ values listed in Table 2, are used in equation (2). Thus, the seismic radii determined from the $\nu_{\rm min0}$ and $\nu_{\rm min1}$ ($R_{\rm sis0}$ and $R_{\rm sis1}$) are computed. The relationship between the $R_{\rm sis1}$ radii obtained in the MS and post-MS and the CESAM model radii ($R_{\rm mod}$) is shown in Fig. 2. In the 1.1 $M_{\odot}$ models, the $R_{\rm sis0}$ and $R_{\rm sis1}$ values are found to be smaller than $R_{\rm mod}$. For both masses, the number of $\nu_{\rm min1}$ data points is greater than that of $\nu_{\rm min0}$. This may be due to the easier detection of the amplitude around $\nu_{\rm min1}$ in the $\Delta\nu$-ν graph, as it is larger. Interestingly, although the radii are derived from MS models, they are much more compatible with post-MS models. We can explain this situation by neglecting the Γ_1 and $\delta\nu_{02}$ in equation (2).

The $\delta\nu_{02}$ refers to the difference in frequencies between two consecutive modes. These modes are influenced by the different physical conditions in the interior structure of the star and are described by different azimuthal quantum numbers (n, l). While n represents the number of nodes in the radial direction, l is related to the depth that the sound wave can reach. When l=0, the wave passes through the core, whereas for l=2, the wave is reflected and returns from the core's outer layers. In main-sequence stars, the value of $\delta\nu_{02}$ is generally large, which means the frequency differences between l=0 and l=2 are noticeable. The $\delta\nu_{02}$ provides information about the core and age of the star. Specifically, it is directly related to the conversion of hydrogen into helium at the core. When hydrogen in the core is converted to helium, the average molecular weight (μ) increases. As μ increases, the speed of sound (c_s) of the star decreases, because the c_s is given by: $c_s \propto \sqrt{P/\rho}$ or $c_s \propto \sqrt{T/\mu}$. The c_s increases with pressure (P) and temperature (T) but decreases with increasing density (ρ). As a star evolves, the c_s decreases significantly due to the expansion of its radius. As a result, the difference between the oscillation frequencies decreases throughout the MS evolution, and a decrease in $\delta\nu_{02}$ is observed. This leads to a smaller frequency difference between l=0 and l=2 in evolved stars. In the subgiant and red giant phases, the differences in interior structures decrease, and mixed modes are observed. This makes it more difficult to detect $\delta\nu_{02}$ in especially in red giants and subgiants. Additionally, as the star evolves, the expansion of the outer layers and the dominance of mixed modes in the interior structure reduce the influence of Γ_1 on oscillation frequencies and small separation. Therefore, the $R_{\rm sis1}$ relation for post-MS stars yields much more consistent results.

Initially, we included models with 0.8 $M_{\odot}$ in the study. These models gave a consistent result with a very small deviation from the $R_{\rm sis1}$=$R_{\rm mod}$ relation in Fig. 2. However, since stars with a mass of 0.8 $M_{\odot}$ are dense (they show significant departures from the ideal gas behavior), the models mostly leave the opacity and equations of state tables. It takes a long time for stars with this mass to complete their main-sequence lifetime (about 20 billion years). 0.8 $M_{\odot}$ models should be considered differently from other models. Therefore, we eliminated models with masses of 0.8 $M_{\odot}$ and studied models with masses of 1.0 and 1.1 $M_{\odot}$ that show solar-like oscillations.

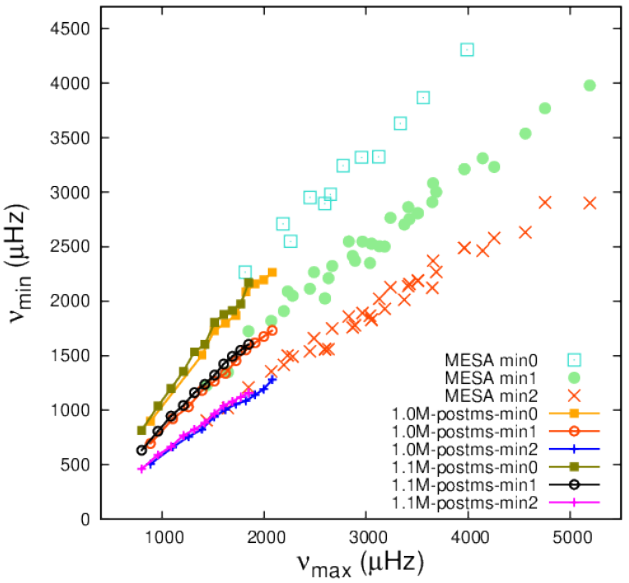

Figure 1. $\nu_{\rm max}$ versus $\nu_{\rm min}$ for post-MS models with different masses. The reference frequencies are compared with the MESA model values. Squares, filled circles, and crosses in the background show min0, min1, and min2 of the MESA model frequencies, respectively.

[2] Gnuplot version 5.4. Available at: http://www.gnuplot.info/

Table 1. Seismic parameters for CESAM MS models. Effective temperatures ($T_{\rm eff}$) and radii are taken from (Marques, Monteiro, & Fernandes 2008). The radii calculated using the Method II for $\nu_{\rm min0}$ and $\nu_{\rm min1}$ are given in the last two columns.

M ($M_\odot$)	R ($R_\odot$)	$T_{\rm eff}$ (K)	$\nu_{\rm max}$ (μHz)	$\nu_{\rm min0}$ (μHz)	$\nu_{\rm min1}$ (μHz)	$\nu_{\rm min2}$ (μHz)	$\Delta\nu$ (μHz)	$\delta\nu_{02}$ (μHz)	$R_{\rm q0}$ ($R_\odot$)	$R_{\rm q1}$ ($R_\odot$)
1	0.91	5639	3701.89	—	2970.12	2288.65	153.87	13.99	—	0.916
1	0.93	5657	3583.45	—	2882.88	2219.10	150.47	13.14	—	0.934
1	0.95	5678	3463.57	—	2797.63	2146.70	146.96	12.27	—	0.952
1	0.96	5696	3341.56	—	2687.18	1957.19	143.53	11.25	—	0.961
1	0.98	5718	3213.28	—	2610.03	1900.86	139.57	10.48	—	0.982
1	1.00	5738	3080.43	3216.26	2528.83	1840.59	135.56	9.57	0.996	1.003
1	1.02	5756	2941.01	3118.55	2442.08	1775.73	131.27	8.66	1.023	1.026
1	1.05	5771	2795.27	3014.27	2349.75	1706.00	126.25	8.00	1.058	1.058
1	1.08	5780	2645.62	2909.33	2254.25	1632.80	121.42	7.09	1.093	1.088
1.1	1.03	5952	3119.08	3484.69	2632.81	1925.58	134.98	13.20	1.040	1.040
1.1	1.05	5965	3020.72	3389.31	2555.22	1873.90	131.98	12.49	1.053	1.054
1.1	1.07	5981	2919.09	3282.84	2475.76	1819.38	128.87	11.76	1.068	1.069
1.1	1.09	5994	2820.22	3184.29	2399.28	1767.36	125.79	11.04	1.084	1.083
1.1	1.11	6005	2716.06	3084.00	2318.84	1712.42	122.36	10.39	1.105	1.102
1.1	1.13	6015	2610.52	2980.46	2232.76	1656.95	118.76	9.72	1.128	1.121
1.1	1.15	6019	2503.88	2879.61	2159.75	1600.56	115.25	9.01	1.153	1.146
1.1	1.18	6021	2394.22	—	2085.89	1542.73	111.44	8.44	—	1.179
1.1	1.21	6020	2283.05	2608.61	2010.55	1483.06	107.67	7.77	1.205	1.214
1.1	1.24	6011	2172.44	2446.24	1909.47	1420.66	103.85	7.10	1.232	1.239
1.1	1.27	5996	2052.19	2378.31	1795.53	1281.77	99.28	6.72	1.276	1.279
1.1	1.32	5987	1917.19	2280.16	1653.78	1193.45	94.462	6.25	1.322	1.315

Table 2. Seismic parameters for CESAM post-MS models and the radii calculated using the Method II for $\nu_{\rm min0}$ and $\nu_{\rm min1}$.

M ($M_\odot$)	R ($R_\odot$)	$T_{\rm eff}$ (K)	$\nu_{\rm max}$ (μHz)	$\nu_{\rm min0}$ (μHz)	$\nu_{\rm min1}$ (μHz)	$\nu_{\rm min2}$ (μHz)	$\Delta\nu$ (μH)	$\delta\nu_{02}$ (μHz)	$R_{\rm q0}$ ($R_\odot$)	$R_{\rm q1}$ ($R_\odot$)
1	1.22	3761	2080.63	2263.97	1731.75	1281.16	101.58	5.40	1.209	1.208
1	1.25	3761	1996.78	2195.60	1676.07	1194.09	98.60	5.22	1.241	1.241
1	1.27	3760	1911.32	2158.04	1617.77	1140.86	95.54	5.19	1.281	1.276
1	1.30	3759	1821.53	2085.61	1552.80	1085.86	92.12	5.35	1.323	1.315
1	1.34	3758	1723.17	1870.37	1452.82	1056.56	88.24	5.48	1.340	1.350
1	1.39	3756	1620.24	1797.49	1337.31	1003.80	84.32	5.51	1.396	1.376
1	1.44	3753	1511.04	1727.48	1265.06	939.45	79.92	—	1.465	1.437
1	1.50	3749	1391.67	1505.90	1179.50	823.78	75.16	—	1.307	1.506
1	1.58	3743	1258.23	—	1030.62	756.80	69.16	—	—	1.574
1	1.70	3730	1105.28	—	921.49	660.93	62.25	—	—	1.715
1	1.94	3699	885.21	898.29	693.59	505.59	51.07	—	1.976	1.963
1	2.56	3679	519.01	—	—	—	33.07	—	—	—
1.1	1.34	3777	1848.39	2168.22	1604.65	1159.27	91.99	—	1.341	1.338
1.1	1.38	3776	1769.45	1973.63	1549.12	1120.13	89.12	—	1.351	1.374
1.1	1.41	3775	1688.74	1913.96	1493.45	1079.78	86.03	—	1.393	1.415
1.1	1.45	3774	1603.60	1878.31	1423.66	1040.63	82.67	—	1.449	1.458
1.1	1.49	3772	1514.31	1806.59	1322.30	967.83	79.25	—	1.501	1.487
1.1	1.54	3770	1419.17	1603.78	1237.42	884.39	75.41	—	1.527	1.536
1.1	1.60	3767	1317.32	1536.02	1161.30	824.60	71.34	—	1.603	1.601
1.1	1.68	3762	1207.94	1356.28	1043.59	768.31	66.53	—	1.666	1.666
1.1	1.77	3755	1086.75	1198.18	945.84	664.38	61.28	—	1.758	1.770
1.1	1.90	3741	959.19	1038.23	806.77	590.81	55.25	—	1.888	1.886
1.1	2.13	3705	799.67	815.12	632.48	460.59	46.55	—	2.116	2.121

3 NEW SCALING RELATION FOR RADIUS AND MASS WITH REFERENCE FREQUENCIES

Determining the mass and radius is crucial for understanding the stellar interior structure and evolution. CESAM model data is particularly useful for radius analysis. However, since the mass range is narrow, MESA models are used in mass analysis. The interior models obtained by Kayhan, Yıldız, & Çelik Orhan (2019) for 20 host stars at different evolutionary stages using the MESA evolution code are very suitable for mass analysis. These stars are solar-like oscillators and reference frequencies can be determined from observational data. The asteroseismic and model parameters determined using oscillation frequencies are taken from Tables 2 and 3 in their study. We divided the models into two different groups as MS and post-MS.

In this section, we derive solutions for the radius and mass based

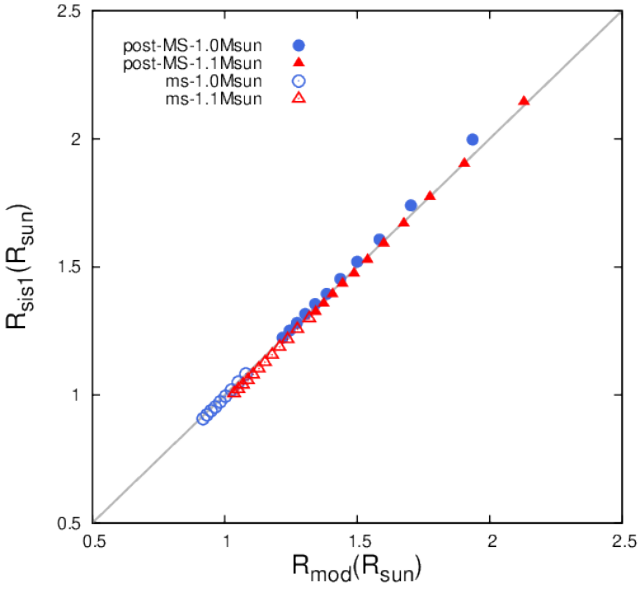

Figure 2. R_{mod} versus computed radius for ν_{min1} (equation 2). Filled circles and triangle indicate post-MS while circles and triangle indicate MS radius, respectively.

on the reference frequencies from the determined MS and post-MS models using two different methods. In Method I, the scaling relations for radius and mass are derived using a logarithmic approach (Eq. 4), whereas Method II uses a quadratic equation (Eq. 7). We derive radius relations using both methods. Since both yield consistent results, we focus on Method I for mass analysis. In the study of Yıldız, Çelik Orhan, & Kayhan (2019), the scaling relations for the mass and radius of the MS stars are determined. While deriving the fitting formulas for the radius and gravity (g), seismic parameters are individually analyzed. In this study, we find the exponents and coefficients of both ν_{min} and $\Delta\nu$ simultaneously.

We can write equation (2) in a more generalized scaling form to determine the radius relation:

$$\frac{R_l}{R_\odot} = 10^a \left(\frac{\nu_{min}}{\nu_{min\odot}}\right)^b \left(\frac{\Delta\nu_\odot}{\Delta\nu}\right)^c . \quad (3)$$

The logarithmic form of this equation is as follows:

$$\log(\frac{R_l}{R_\odot}) = a + b\log\left(\frac{\nu_{min}}{\nu_{min\odot}}\right) + c\log\left(\frac{\Delta\nu_\odot}{\Delta\nu}\right). \quad (4)$$

Equation (4) is an equation with two variables and three unknowns:

$$f(x,y) = a + bx + cy. \quad (5)$$

The values of a, b and c for MS and post-MS obtained from the simultaneous solution of the function $f(x,y)$ for $x = \nu_{min}/\nu_{min\odot}$ and $y = \Delta\nu_\odot/\Delta\nu$ are given in Table 4. In the derived relations, the solar seismic values listed in Table 3 are used.

The two-variable, five-unknown g(x,y) function defined to obtain the radius with the Method II is:

$$g(x,y) = p + qx + rx^2 + sy + ty^2. \quad (6)$$

The quadratic form of this equation is as follows:

$$\frac{R_q}{R_\odot} = p + q\left(\frac{\nu_{min}}{\nu_{min\odot}}\right) + r\left(\frac{\nu_{min}}{\nu_{min\odot}}\right)^2 + s\left(\frac{\Delta\nu_\odot}{\Delta\nu}\right) + t\left(\frac{\Delta\nu_\odot}{\Delta\nu}\right)^2 \quad (7)$$

Table 3. Asteroseismic solar parameters. ν_{max} and $\Delta\nu_\odot$ are from (Huber et al. 2011), the reference frequency $\delta\nu_{02\odot}$ is from (Yıldız, Çelik Orhan, & Kayhan 2016).

Solar asteroseismic parameters		References
$\nu_{max\odot}$	3090 ± 30 μHz	(Huber et al., 2011)
$\Delta\nu_\odot$	135.1 ± 0.1 μHz	
ν_{min0}	3256.6 ± 32.6 μHz	(Yıldız et al., 2016)
ν_{min1}	2555.2 ± 25.6 μHz	
ν_{min2}	1879.5 ± 18.8 μHz	
$\delta\nu_{02\odot}$	9.8 ± 0 μHz	

Table 4. Coefficients and uncertainties of radii determined by Method I from CESAM models.

MS		
Coefficients	R_{l0}	R_{l1}
a	0.0035 ± 0.0012	0.0058 ± 0.0007
b	0.382 ± 0.051	0.591 ± 0.085
c	1.152 ± 0.059	1.423 ± 0.097
post-MS		
a	-0.0060 ± 0.0035	0.0006 ± 0.0015
b	0.341 ± 0.071	0.484 ± 0.041
c	1.162 ±0.096	1.334 ± 0.054

Table 5. Coefficients and uncertainties of radii determined by the Method II from CESAM models

MS		
Coefficients	R_{q0}	R_{q1}
p	-0.924 ± 0.256	-2.413 ± 0.276
q	-0.185 ± 0.665	3.765 ± 0.753
r	0.314 ± 0.341	-1.496 ± 0.360
s	2.376 ± 0.430	0.742 ± 0.515
t	-0.576 ± 0.194	0.420 ± 0.255
post-MS		
p	-1.424 ± 0.467	-2.194 ± 0.304
q	2.188 ± 0.831	3.662 ± 0.537
r	-1.196 ± 0.676	-2.170 ± 0.455
s	1.451 ± 0.267	1.628 ± 0.174
t	-0.136 ± 0.055	-0.140 ± 0.035

Although Method II introduces some corrections for the radius, the results are consistent with Method I. Therefore, only one of the methods is selected. The relation determined by Method II for the radius is used. The values of p, q, r, s, t for the MS and post-MS radii (R_{q0} and R_{q1}) obtained from the simultaneous solution of the function $g(x,y)$ are given in Table 5. The radii R_{q0} and R_{q1} are plotted against R_{mod} in Figure 3. Although the ν_{min0} data of the 1.0 $M_\odot$ models are not available numerically in both graphs, the radius calculations of the post-MS models give quite compatible results for ν_{min0} and ν_{min1}. This shows us how precise calculations we can make with the scaling relations using seismic parameters. In addition, the fit between radii is quite successful, including the models with 1.1 $M_\odot$.

Highly accurate, direct relations based on reference frequencies

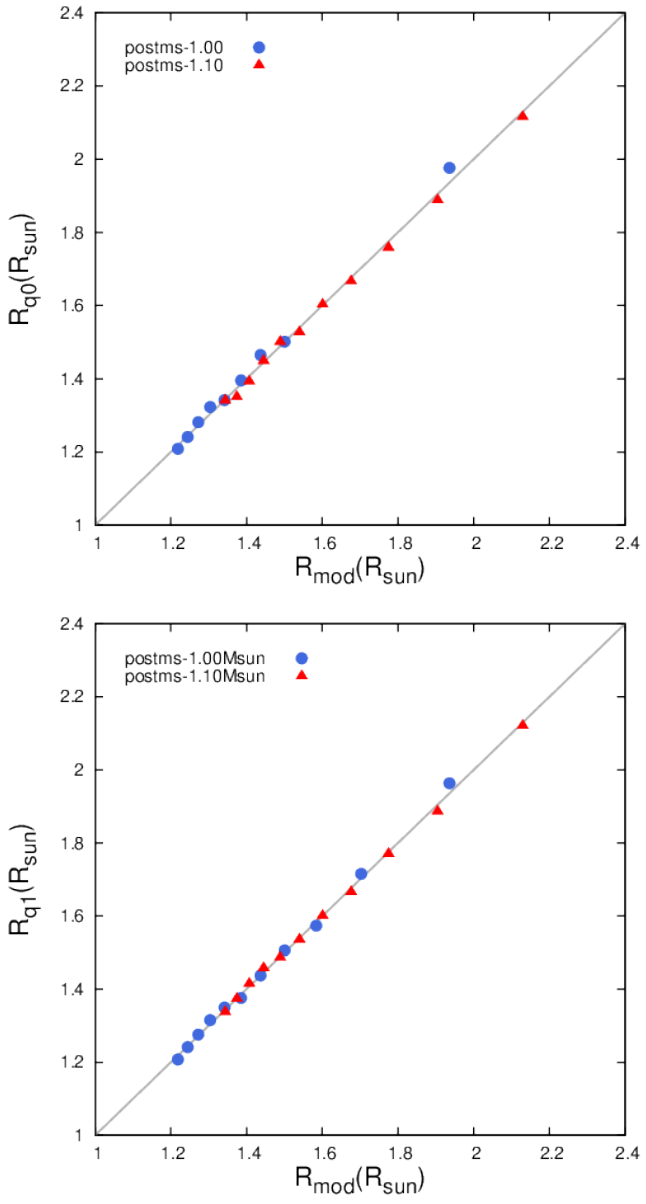

Figure 3. R_{q0}-R_{mod} and R_{q1}-R_{mod} are plotted from post-MS CESAM models. Filled circles indicate post-MS 1.0 $M_\odot$ radii while filled triangle indicate post-MS 1.1 $M_\odot$ radii. Radii are plotted in the same range (1.22-2.13 $R_\odot$) in solar units.

cannot be obtained for the mass. In order to obtain an explanation for the mass, first of all, it is necessary to determine g and R well. We can compute the seismic mass (M_{sis}) by deriving the relations for g and R from the seismic data of the models:

$$\frac{M_{sis}}{M_\odot} = \left(\frac{g_{sis}}{g_\odot}\right)\left(\frac{R_{sis0}}{R_\odot}\right)^2 . \quad (8)$$

To determine the mass, we use MESA models in the mass range of 1.07-1.55 $M_\odot$. These models include subgiant stars. Microscopic diffusion is included in the constructing of models with $M < 1.2$ $M_\odot$. For $M > 1.2$ $M_\odot$, it is not included. The Z_{0mod} parameter in Table 2 of Kayhan, Yıldız, & Çelik Orhan (2019) is the initial Z (Z_0) value. The CESAM models are constructed for the same composition and those with available frequencies are limited to 1.0 and 1.1 $M_\odot$.

Table 6. Coefficients and uncertainties for R and g from MESA post-MS models, determined by Method I.

Coefficients	R_{l0}	R_{l1}
k	-0.0066 ± 0.0079	-0.0071 ± 0.0100
l	0.191 ± 0.042	0.211 ± 0.062
m	0.964 ± 0.035	0.997 ± 0.054
n	0.063 ± 0.018	0.068 ± 0.020
	g_{l0}	g_{l1}
k'	-0.0004 ± 0.0179	0.0142 ± 0.0119
l'	0.346 ± 0.095	0.498 ± 0.074
m'	-0.893 ± 0.078	-0.731 ± 0.064
n'	0.039 ± 0.040	0.016 ± 0.024

On the other hand, the MESA models are constructed for a wider mass range and for different compositions. Z ranges from 0.012 to 0.026. Model parameters such as g and R are also known to show a slight dependence on Z. Therefore, we use the 3-variable function $f(x, y, t)$ instead of the two-variable $f(x, y)$ in equation (5). For this we define the parameter t:

$$t = \frac{Z_0}{Z_\odot} + 0.1 \quad (9)$$

The solar metallicity is taken to be $Z_\odot = 0.0134$ (Asplund et al. 2009). We added the term 0.1 to account for stars with Z values of 0 or very small. Then, we separately derived the simultaneous solutions of 3-variable (ν_{min}, $\Delta\nu$ and Z_{mod}) from the MS and post-MS models with the Method I for g_l and R_l:

$$\frac{g_l}{g_\odot} = 10^{k'}\left(\frac{\nu_{min}}{\nu_{min\odot}}\right)^{l'}\left(\frac{\Delta\nu_\odot}{\Delta\nu}\right)^{m'}\left(\frac{Z_0}{Z_\odot}+0.1\right)^{n'} , \quad (10)$$

$$\frac{R_l}{R_\odot} = 10^{k}\left(\frac{\nu_{min}}{\nu_{min\odot}}\right)^{l}\left(\frac{\Delta\nu_\odot}{\Delta\nu}\right)^{m}\left(\frac{Z_0}{Z_\odot}+0.1\right)^{n} . \quad (11)$$

The coefficients for R_l and g_l along with their uncertainties, are listed in Table 6. The model gravity (g_{mod}) is plotted against g_l calculated from ν_{min0} and ν_{min1} in Fig.4, and R_{mod} plotted against R_l in Fig. 5 are shown. The agreement of gravity and radii with the model values is very clear. This is extremely important for us to determine the mass precisely. The logarithmically derived relations for g and R show a good agreement with the MS models. However, the results obtained using ν_{min1} provide a slightly better fit for both parameters. Additionally, for the scaling relations of mass and radius in MS stars (e.g., see Yıldız, Çelik Orhan, & Kayhan 2019).

In this study, we mainly focus on the M and R relations of post-MS stars. This study presents the first model-based derivation of the mass relation for post-MS stars. Consequently, we compute the masses M_{l0} and M_{l1} using ν_{min0} and ν_{min1}. The model mass (M_{mod}) versus M_{l0} and M_{l1} is plotted in Fig. 6. The masses and radii obtained closely match the post-MS model values. Similar to the MS models, the results derived from ν_{min1} provide a better improvement. Because in general, the amplitude around ν_{min1} is much deeper than that around ν_{min0}, allowing for a more precise determination of ν_{min1} between the reference frequencies. Therefore, we predict that the radii and masses calculated with ν_{min1} will give more accurate results.

4 RESULTS AND DISCUSSIONS

In this study, we take a comprehensive approach by integrating modeling, theoretical, and observational data. This allows us to compare

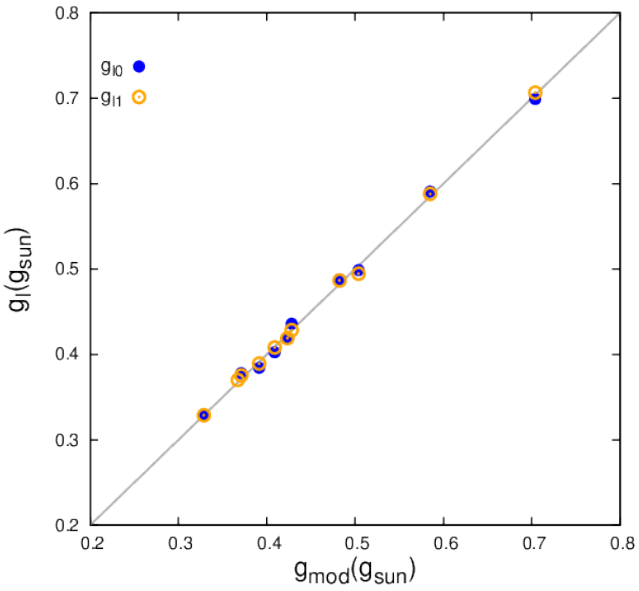

Figure 4. g_{l0} and g_{l1} are plotted with respect to $g_{\rm mod}$. The filled circles are for the gravity computed for $\nu_{\rm min0}$ and the circles are for the gravity computed for $\nu_{\rm min1}$.

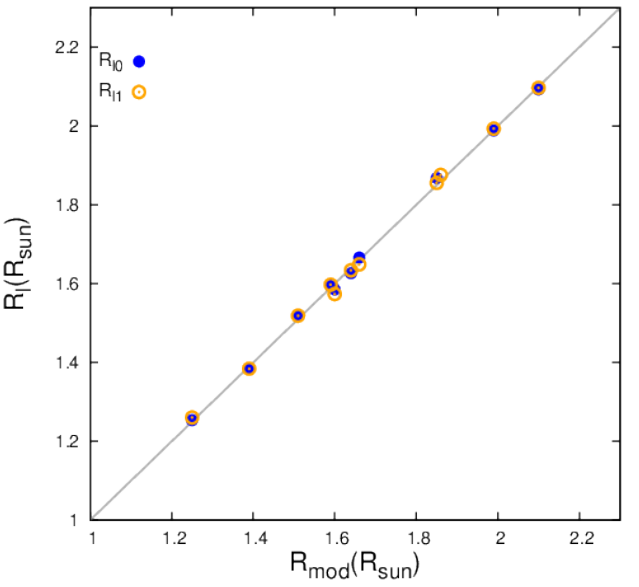

Figure 5. R_{l0} and R_{l1} are plotted with respect to $R_{\rm mod}$. Filled circles indicate the radii computed for $\nu_{\rm min0}$, while circles indicate the radii computed for $\nu_{\rm min1}$. Radii range from 1.2-2.2 $R_\odot$.

the observed frequencies of the star with the frequencies obtained from models using different input parameters. Furthermore, we can evaluate how well the M and R relations derived from models agree with the observed M and R values. In this section, we mainly apply the relations we obtained for post-MS stars to KL stars. The data for these stars are taken from Table B1 in Yıldız, Çelik Orhan, & Kayhan (2019). The radii $R_{\rm sis0}$ and $R_{\rm sis1}$ in Table B1 are referred to as R_0 and R_1 in this study, respectively. Similarly, $M_{\rm sis0}$ is defined as

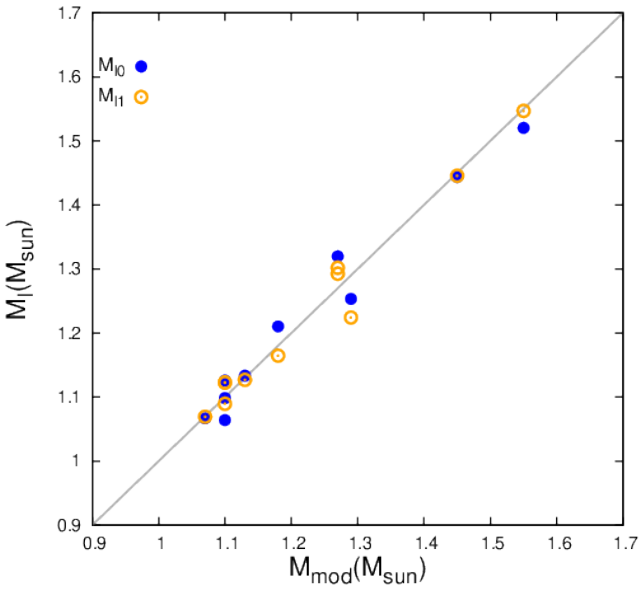

Figure 6. M_{l0} and M_{l1} are plotted with respect to $M_{\rm mod}$. The filled circles represent the masses computed for $\nu_{\rm min0}$, while the open circles correspond to masses computed for $\nu_{\rm min1}$. The masses are plotted in the range of 1.01-1.55 $M_\odot$ in all MESA post-MS models.

M_0 and $M_{\rm sis1}$ as M_1. Table B1 are analyzed separately for MS and post-MS stars.

In the previous section, we derived the mass and radius relations for post-MS stars for the first time using both Method I and Method II. Since both methods yielded similar results, we chose Method II for radius determination and Method I for mass estimation. The new mass and radius values obtained using these methods are presented in Table 7 along with their uncertainties. The uncertainties in mass and radius are estimated by Monte Carlo simulations using the observed values of $\Delta\nu$, $\nu_{\rm min0}$, $\nu_{\rm min1}$, and Z. In the simulation, 10000 synthetic data points are generated for each parameter within its observational uncertainty range, assuming a Gaussian distribution. For each star, 10000 mass and radius values are computed based on these synthetic samples. The 1 σ uncertainties in mass (σ_M) and radius (σ_R) are then derived as the standard deviations of these distributions.

4.1 Radius of the Kepler Legacy stars

The scaling relations for R based on $\nu_{\rm min0}$ and $\nu_{\rm min1}$ are derived from CESAM and MESA models using Methods I and II. In this section, we apply these R relations to MS and post-MS KLs, and obtain the radii as $R_{\rm q0}$, $R_{\rm q1}$ and $R_{\rm l0}$, $R_{\rm l1}$, respectively.

4.1.1 MS Kepler Legacy stars

First, we apply the scaling relation for the radius obtained with Method I from the CESAM MS models using KLs. Using this method, the relation between $R_{\rm q0}$ determined for $\nu_{\rm min0}$ and R_0 is plotted logarithmically in Figure 7a. Generally, there is a good correlation between the two radii, but an increasing deviation is noticeable for radii larger than 1.5 $R_\odot$. This deviation is especially apparent for stars with masses greater than 1.15 $M_\odot$. In this study, the R relations obtained from the CESAM models are based on the 1.0 and 1.1 $M_\odot$ models. The red circles highlight stars in the 0.95–1.15 M⊙ range,

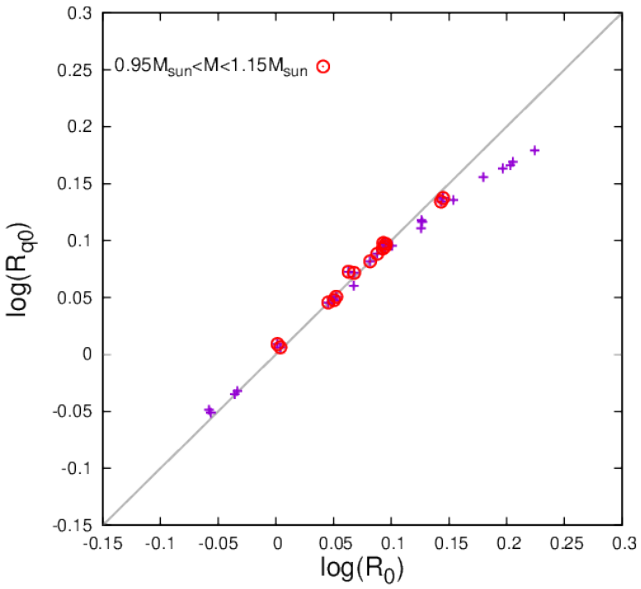

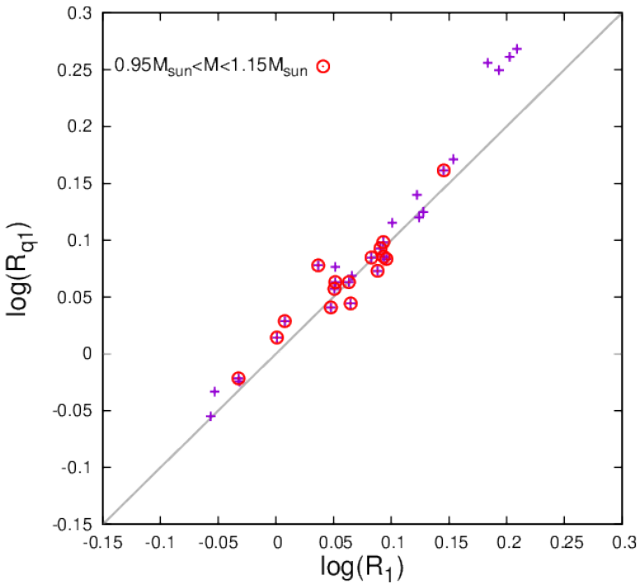

Figure 7. R_q is plotted with respect to MS KLs radius. a) R_{q0} versus R_0. b) R_{q1} versus R_1. Radii are plotted logarithmically (plus). The red circles show KLs in the narrow mass range of 0.95-1.15 $M_\odot$ for which CESAM models are available.

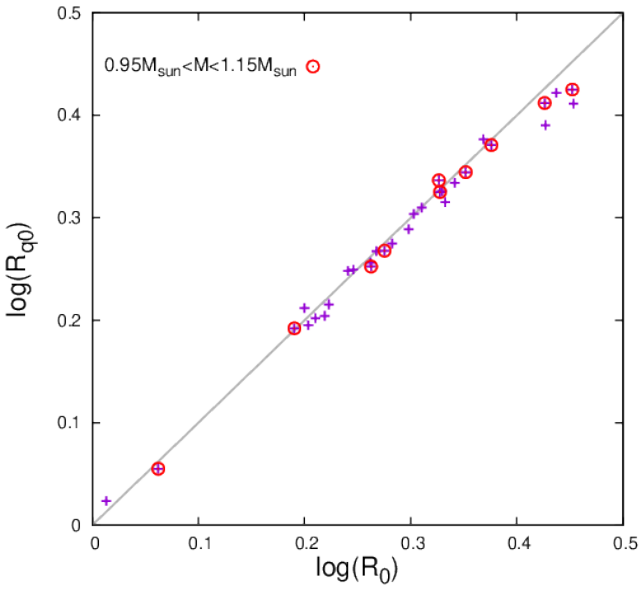

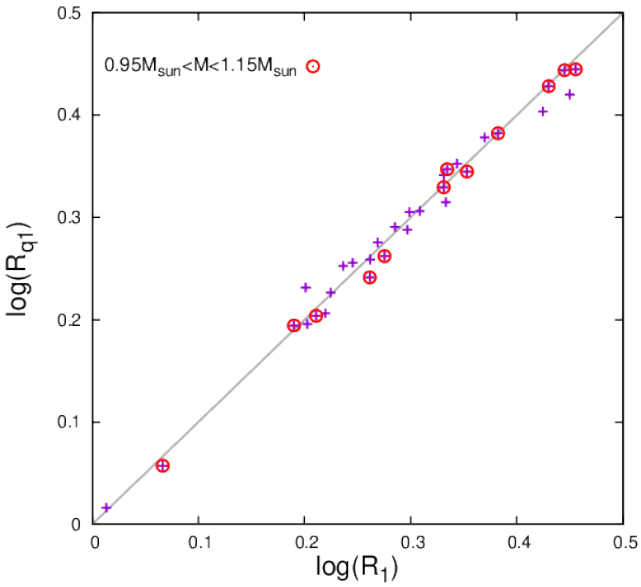

Figure 8. R_q is plotted logarithmically with respect to post-MS KLs radius. a) R_{q0} versus R_0. b) R_{q1} versus R_1. The red circles represent Kepler Legacy stars with masses falling within the CESAM model range of 0.95 to 1.15 $M_\odot$.

for which the agreement between Rq0 and R_0 is significantly better than for stars outside this mass range.

Then, as a second step, we apply the relation determined from equation (7) to KLs and obtain the radius R_{q1}. The relationship between R_1 and R_{q1} is shown in Fig. 7b. As in Fig. 7, a deviation after 1.5 $R_\odot$ is also noticeable in this graph. This is because the masses of the MS models we used are very limited compared to the mass range of the selected KLs.

4.1.2 *post-MS Kepler Legacy stars*

In this section, we apply the radius relations for ν_{min0} and ν_{min1}, derived from post-MS models using Methods I and II, to KL stars. The radii determined by both methods are listed in Table 7. The radii in Table 7, R_{l0} and R_{l1} are obtained from equation (11), while R_{q0} and R_{q1} are computed using equation (7). For the KL subgiant stars, the radii determined by Method I range between 1.05 and 2.94 $R_\odot$, whereas those determined by Method II lie within the range 1.06 to 2.66 $R_\odot$.

The radius R_{q0} is plotted logarithmically against R_0 in Fig. 8a. The radius R_{q0} agrees very well with the radius R_0. Additionally, the radius range of the post-MS models in the mass range (0.95-1.15 $M_\odot$) covers almost the entire range of radii of Kepler subgiant stars. A small deviation is noticeable for radii larger than 2.4 $R_\odot$, although overall agreement remains strong. R_{q1} versus R_1 is as in Fig. 8b. The radii are well matched for the specified mass range. The small difference after 2.4 $R_\odot$ in Fig 8a decreases here. This shows that

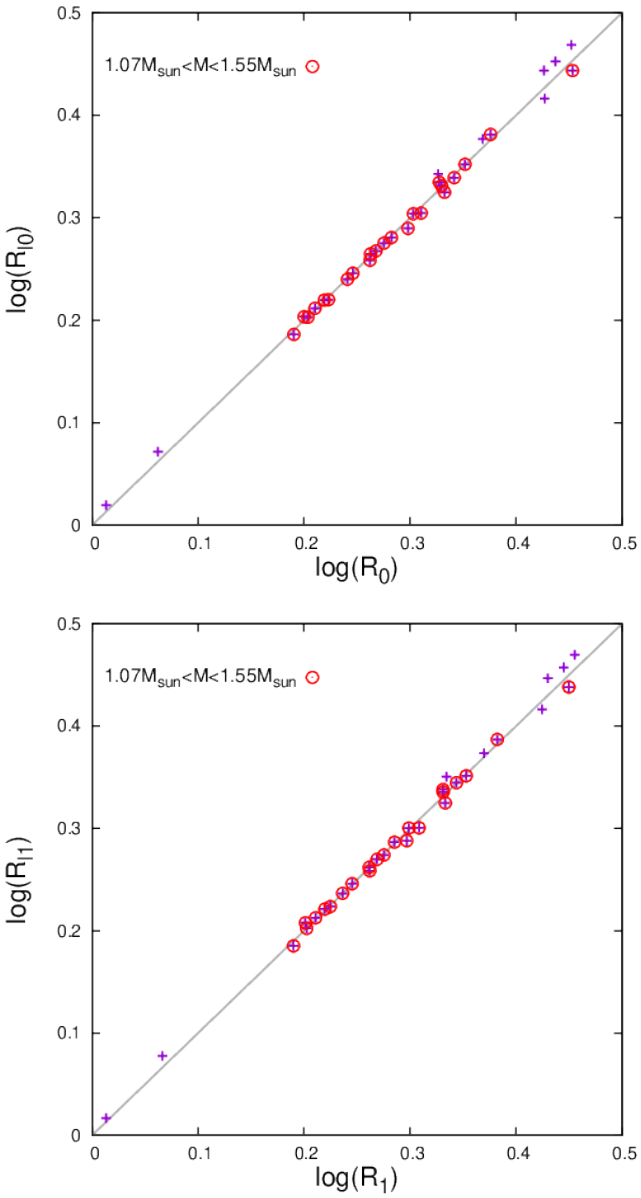

Figure 9. R_l versus post-MS KLs radii. Radii are plotted logarithmically. a)R_{l0} is plotted with respect to R_0. b)R_{l1} is plotted with respect to R_0. The red circles show KLs in the mass range of 1.07-1.55 $M_\odot$ for which MESA models are available.

the scaling relation for the radius derived from the CESAM post-MS models can be determined much more accurately for $\nu_{\rm min1}$ than for $\nu_{\rm min0}$.

The scaling relations for R, derived from MESA post-MS models covering a wide mass range, are presented in Section 3. Based on these relations, the post-MS radii R_0 and R_1, corresponding to the computed R_{l0} and R_{l1} for $\nu_{\rm min0}$ and $\nu_{\rm min1}$, are plotted in Fig. 9, respectively. The obtained radii appear to be in good agreement with the KLs radii. Moreover, while they are similar to the radii determined from CESAM models, they offer a more precise match to the observed values.

4.2 Mass of the Kepler Legacy stars

In this section, we apply the M_l solutions, derived from MESA MS and post-MS models using Method I, to the KLs. The description for mass determination from MESA models with Method I is given in Section 3. As a key contribution of this study, we derive for the first time a scaling relation for mass based on post-MS models. Finally, the results obtained from the MS models are compared with previous studies.

4.2.1 MS Kepler Legacy stars

A previous study Yıldız, Çelik Orhan, & Kayhan (2019) applied solutions derived from MS models to the KLs. In their method, the parameters $\Delta\nu$ and $\nu_{\rm min}$ are initially calibrated, after which a Z correction was applied. In this study, we obtain a simultaneous solution for the parameters $\Delta\nu$, $\nu_{\rm min}$, and $Z_{\rm mod}$. We apply the M_l solutions derived using Method I to the KLs and compute the corresponding masses M_{l0} and M_{l1}. The relationships between these model-based masses and the KLs masses are as follows:

$$M_{l0} = (1.0060 \pm 0.0014) M_0, \tag{12}$$

$$M_{l1} = (1.0140 \pm 0.0011) M_1. \tag{13}$$

The results show high consistency for both solutions. Since the multiplier of M_0 (1.006) is very close to unity, M_{l0} shows significantly better agreement with M_0. However, when uncertainties are taken into account, M_{l1} appears to yield more reliable results. Accordingly, we can predict that the relationships for the radii will be much better. M_{l0} versus M_0 is plotted in Fig. 10a and M_{l1} versus M_1 is plotted in Fig. 10b. Despite some scatter, Fig. 10 shows good consistency with the results of Yıldız, Çelik Orhan, & Kayhan (2019), while also improving upon their method through the use of a three-variable simultaneous solution for g and R in the determination of M.

4.2.2 post-MS Kepler Legacy stars

In this section, we obtain the scaling relation for M from MESA post-MS models for the first time and apply it to KLs. We determine the masses M_{l0} and M_{l1}. The relationships between these masses and the KLs masses are as follows:

$$M_{l0} = (0.998 \pm 0.012) M_0, \tag{14}$$

$$M_{l1} = (0.998 \pm 0.008) M_1. \tag{15}$$

When comparing equation (14) with equation (15), the masses determined from M_{l0} and M_{l1} yield nearly identical results. This shows that the asteroseismic masses of post-MS stars can be determined quite accurately. The graph of M_{l0} versus M_{l1} is plotted in Fig. 11 .The calculated masses are given in Table 7. The post-MS models M_{l0} and M_{l1} masses agree quite well with each other. However, the masses derived from the scaling relation based on $\nu_{\rm min1}$ provide a slight improvement compared to those determined from $\nu_{\rm min0}$. This can be explained as follows: these stars are evolved stars that have separated from the main sequence. As stars evolve, the depth of the $\nu_{\rm min0}$ frequency gradually decreases and eventually becomes undetectable in advanced evolutionary stages. On the other hand, the $\nu_{\rm min1}$ frequency, similar to MS stars, is much deeper compared to other minima in post-MS stars as well.

Table 7. Asteroseismic parameters post-MS Kepler legacy stars. The KIC ID of each star is given in the first column. $\nu_{\rm max}$, $\nu_{\rm min0}$, $\nu_{\rm min1}$, $\nu_{\rm min2}$, $\nu_{\rm min1}$, $\Delta\nu$, $\delta\nu_{02}$, $T_{\rm eS}$ (effective temperatures from spectra), M_0, M_1, R_0, and R_1 are from (Yıldız, Çelik Orhan, & Kayhan 2019).M_0, M_1, R_0, and R_1 correspond to $M_{\rm sis0}$, $M_{\rm sis1}$, $R_{\rm sis0}$, and $R_{\rm sis1}$, respectively. The fundamental parameters $M_{\rm l0}$, $M_{\rm l1}$, $R_{\rm l0}$, and $R_{\rm l1}$ are obtained by Method I, while $R_{\rm q0}$ and $R_{\rm q1}$ are computed by Method II.

KIC ID	$\nu_{\rm max}$ (μHz)	$\nu_{\rm min0}$ (μHz)	$\nu_{\rm min1}$ (μHz)	$\nu_{\rm min2}$ (μHz)	$\Delta\nu$ (μHz)	$\delta\nu_{02}$ (μHz)	T_{eS} (K)	M_0 ($M_\odot$)	M_1 ($M_\odot$)	R_0 ($R_\odot$)	R_0 ($R_\odot$)	$M_{\rm l0}$ ($M_\odot$)	M_1 ($M_\odot$)	$R_{\rm l0}$ ($R_\odot$)	$M_{\rm l1}$ ($R_\odot$)	$R_{\rm q0}$ ($R_\odot$)	$R_{\rm q1}$ ($R_\odot$)
1435467	1324	1626.4	1274	0	70.9	4.8	6264	1.24	1.27	1.65	1.66	1.24	1.29	1.66	1.67	1.64	1.68
												0.02	0.02	0.06	0.07	0.02	0.02
3424541	745	1046.6	755.4	0	41.1	4.7	6165	1.80	1.74	2.65	2.64	1.63	1.62	2.61	2.61	2.46	2.53
												0.08	0.08	0.40	0.42	0.05	0.06
3632418	1159	1370.9	1055	0	60.4	3.8	6148	1.24	1.26	1.83	1.83	1.25	1.28	1.85	1.86	1.85	1.89
												0.05	0.05	0.12	0.13	0.01	0.02
5955122	861	952.7	717.9	0	49.4	4.8	5952	1.20	1.21	2.12	2.13	1.21	1.18	2.11	2.11	2.07	2.06
												0.06	0.06	0.22	0.23	0.04	0.04
6508366	926	1267.5	978.3	672.2	51.5	3.3	6354	1.43	1.46	2.11	2.12	1.42	1.49	2.14	2.16	2.12	2.19
												0.03	0.03	0.14	0.15	0.03	0.04
6603624	2402	2529.7	2080.5	0	109.7	5.5	5625	0.98	1.03	1.14	1.15	1.08	1.15	1.18	1.20	1.14	1.14
												0.02	0.03	0.04	0.05	0.02	0.02
6679371	908	1284.8	1000.6	725.8	50.6	4.1	6344	1.51	1.55	2.17	2.18	1.46	1.55	2.18	2.21	2.16	2.25
												0.07	0.07	0.20	0.22	0.03	0.03
6933899	1391	1538.7	1178	0	71.8	4.9	5837	1.14	1.15	1.61	1.61	1.19	1.19	1.63	1.63	1.59	1.60
												0.05	0.05	0.11	0.12	0.03	0.03
7103006	1124	1432.9	1134.4	790.3	60.1	4.5	6394	1.36	1.41	1.90	1.91	1.36	1.44	1.91	1.93	1.88	1.95
												0.03	0.04	0.12	0.13	0.03	0.04
7799349	561	580.6	448.6	0	33.2	3.4	4954	1.03	1.08	2.63	2.66	1.22	1.22	2.78	2.80	2.58	2.68
												0.06	0.06	0.33	0.36	0.02	0.02
7976303	851	1036.3	754	0	51	4.5	6053	1.15	1.13	2.02	2.01	1.14	1.10	2.02	2.00	2.04	2.02
												0.02	0.02	0.09	0.10	0.02	0.03
8026226	545	687.7	479.1	0	34.6	3.6	6230	1.39	1.32	2.80	2.78	1.35	1.25	2.78	2.74	2.58	2.63
												0.03	0.03	0.26	0.26	0.03	0.04
8228742	1171	1375.9	1036.9	0	62	4.8	6042	1.24	1.23	1.81	1.81	1.23	1.23	1.81	1.81	1.80	1.81
												0.02	0.02	0.07	0.07	0.02	0.02
8524425	1081	1128	831.3	0	59.4	5	5634	1.07	1.05	1.81	1.81	1.15	1.09	1.84	1.83	1.79	1.74
												0.02	0.02	0.07	0.07	0.02	0.02
8561221	491	488	370.5	0	29.8	2.4	5245	0.99	1.04	2.80	2.82	1.16	1.14	2.94	2.95	2.66	2.78
												0.02	0.02	0.10	0.10	0.00	0.01
8694723	1384	1661.8	1261.7	0	74.9	5.4	6258	1.10	1.09	1.53	1.53	1.10	1.11	1.54	1.53	1.56	1.56
												0.05	0.05	0.09	0.09	0.02	0.02
8702606	664	688.7	554.5	0	39.7	3.5	5540	1.03	1.12	2.34	2.38	1.14	1.17	2.41	2.44	2.35	2.41
												0.02	0.02	0.15	0.16	0.02	0.03
8760414	2384	2628.3	2041.6	0	117.1	5.6	5850	0.85	0.85	1.03	1.03	0.87	0.89	1.05	1.04	1.06	1.04
												0.07	0.06	0.06	0.07	0.00	0.01
9574283	455	459.3	370.6	0	29.9	3	5120	0.90	0.99	2.72	2.77	1.04	1.07	2.83	2.87	2.64	2.78
												0.03	0.04	0.43	0.46	0.03	0.04
9812850	1195	1558	1171.2	877.2	65.1	4.1	6258	1.26	1.25	1.74	1.74	1.27	1.28	1.76	1.76	1.78	1.80
												0.06	0.06	0.14	0.15	0.03	0.04
10018963	987	1168.7	866	0	55.2	5.1	6145	1.23	1.21	1.96	1.96	1.21	1.18	1.95	1.94	1.94	1.94
												0.05	0.05	0.14	0.15	0.02	0.02
10162436	968	1370.4	977	671.1	55.5	3.6	6149	1.39	1.32	1.98	1.97	1.37	1.34	2.01	2.00	2.01	2.02
												0.06	0.06	0.17	0.18	0.03	0.03
10355856	1330	1823.7	1308.8	0	68.1	4.7	6351	1.38	1.30	1.72	1.70	1.35	1.34	1.74	1.72	1.77	1.79
												0.06	0.06	0.11	0.12	0.02	0.02
10920273	1024	1103.1	826.6	0	57.1	4.9	5710	1.09	1.09	1.86	1.86	1.15	1.11	1.88	1.88	1.85	1.83
												0.02	0.02	0.08	0.08	0.02	0.03
11244118	1420	1526.8	1169.9	0	71.3	5.5	5745	1.20	1.21	1.65	1.65	1.23	1.23	1.66	1.66	1.60	1.61
												0.02	0.02	0.07	0.07	0.02	0.03
11253226	1638	2150.4	1684.6	1194.6	76.9	4.4	6410	1.35	1.37	1.56	1.57	1.35	1.46	1.60	1.61	1.63	1.70
												0.06	0.06	0.10	0.11	0.02	0.03
11395018	834	875.3	685.2	0	47.3	4.2	5445	1.06	1.11	2.10	2.12	1.18	1.19	2.16	2.18	2.11	2.14
												0.02	0.02	0.10	0.11	0.02	0.03
11414712	707	781.2	586.9	0	43.9	4.1	5635	1.07	1.08	2.22	2.22	1.14	1.10	2.25	2.25	2.21	2.21
												0.02	0.03	0.16	0.17	0.03	0.04
11717120	585	583.7	434.3	0	37.8	4.2	5150	0.86	0.88	2.32	2.32	0.99	0.94	2.38	2.36	2.38	2.39
												0.03	0.03	0.27	0.28	0.04	0.05
12258514	1440	1667.1	1251.8	0	74.5	4.9	5990	1.19	1.18	1.58	1.58	1.21	1.20	1.60	1.59	1.57	1.57
												0.02	0.02	0.05	0.06	0.02	0.02
12508433	793	786.7	650.6	0	44.9	3.8	5134	0.94	1.04	2.09	2.13	1.12	1.18	2.20	2.24	2.17	2.22
												0.06	0.06	0.24	0.26	0.03	0.04

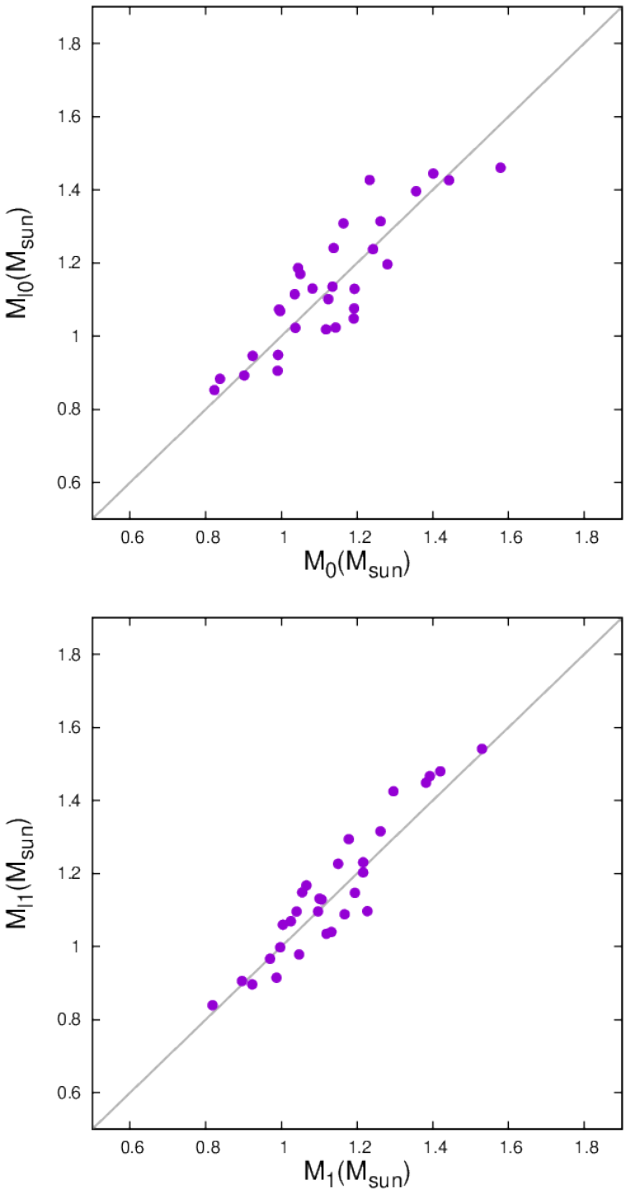

Figure 10. M_1 mass versus observational Kepler mass for MS stars. a)M_{l0} is plotted with respect to M_0. b)M_{l1} is plotted with respect to M_0.

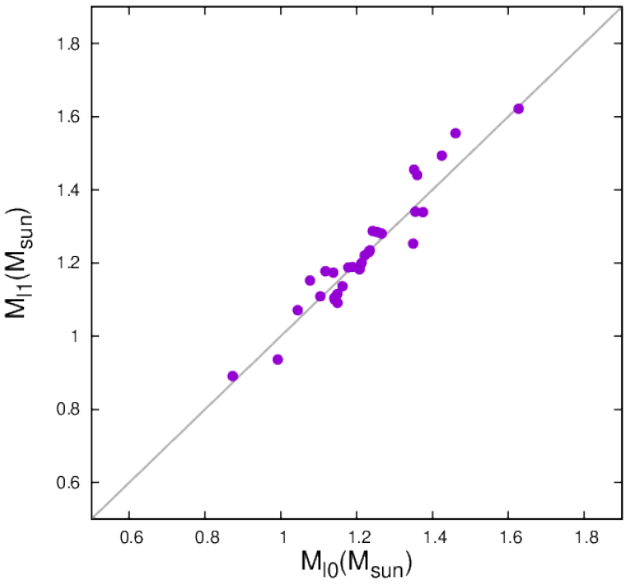

Figure 11. M_{l0} is plotted with respect to M_{l1} for post-MS Kepler stars.

5 CONCLUSIONS

Determining the masses and radii of stars with high precision is crucial for understanding the physical processes occurring in their interiors. By using the oscillation frequencies of solar-like oscillating stars, highly accurate solutions for mass and radius can be obtained. In this study, we analyze the oscillation frequencies of stellar models obtained using the CESAM and MESA evolution codes and derive new scaling relations for M and R. The primary aim of this study is to determine whether the scaling relations obtained from the models are model dependent. The fact that both the CESAM and MESA codes yield almost identical relations indicates that the obtained relations are model-independent. While our analysis includes MS stars, the main focus is on determining the M and R relations of post-MS stars.

In this paper, we analyzed the oscillation frequencies of the CESAM 1.0 and 1.1 $M_\odot$ models, determining $\Delta\nu$, $\delta\nu_{02}$ and reference frequencies. Using these reference frequencies $\nu_{\rm min0}$ and $\nu_{\rm min1}$, we derived solutions for R from MS and post-MS models. We applied two different approaches to determine the radii and masses: the logarithmic method (Method I) and the quadratic method (Method II). In particular, this study presents, for the first time, a radius scaling relation derived from post-MS models. Although Method II introduced some corrections, the results are highly consistent with those obtained using Method I. This indicates that the scaling relations derived from the seismic data are independent of the method used.

Furthermore, we derived the g and R relations to determine the masses of MS and post-MS stars from the MESA models. A scaling relation for the mass of post-MS stars was obtained for the first time. In determining M, we also obtain a simultaneous solution for the parameters $\Delta\nu$, $\nu_{\rm min}$, and $Z_{\rm mod}$. Our results are compared with previous studies and showed strong consistency with the literature.

Finally, the mass and radius scaling relations derived from both evolution codes are applied to Kepler Legacy stars. The seismic solutions based on $\nu_{\rm min}$ show excellent agreement with the Kepler data. These findings demonstrate that the fundamental parameters of evolved solar-like stars can be reliably determined using the proposed scaling relations. In future research, these scaling relations can be derived for stars with a wider range of masses, radii, and metallicities. Future studies may extend these relations to a wider range of stellar masses, radii, and metallicities. Moreover, their accuracy can be further evaluated using data from space missions such as TESS and Kepler.

ACKNOWLEDGEMENTS

This work is supported by the Scientific and Technological Research Council of Turkey (TÜBİTAK: 123F019). This study is part of the author's MSc thesis submitted to Ege University.

REFERENCES

Aerts C., 2021, RvMP, 93, 015001. doi:10.1103/RevModPhys.93.015001

Alexander D. R., Ferguson J. W., 1994, ApJ, 437, 879. doi:10.1086/175039

Angulo C., Arnould M., Rayet M., Descouvemont P., Baye D., Leclercq-Willain C., Coc A., et al., 1999, NuPhA, 656, 3. doi:10.1016/S0375-9474(99)00030-5

Asplund M., Grevesse N., Sauval A. J., Scott P., 2009, ARA&A, 47, 481. doi:10.1146/annurev.astro.46.060407.145222

Baglin A., Auvergne M., Barge P., Deleuil M., Catala C., Michel E., Weiss W., et al., 2006, ESASP, 1306, 33.

Borucki W. J., Koch D., Basri G., Batalha N., Brown T., Caldwell D., Caldwell J., et al., 2010, Sci, 327, 977. doi:10.1126/science.1185402

Böhm-Vitense E., 1958, ZA, 46, 108

Brown T. M., Gilliland R. L., Noyes R. W., Ramsey L. W., 1991, ApJ, 368, 599. doi:10.1086/169725

Chaplin W. J., Kjeldsen H., Christensen-Dalsgaard J., Basu S., Miglio A., Appourchaux T., Bedding T. R., et al., 2011, Sci, 332, 213. doi:10.1126/science.1201827

Christensen-Dalsgaard J., 2008, Ap&SS, 316, 113. doi:10.1007/s10509-007-9689-z

Cyburt R. H., Amthor A. M., Ferguson R., Meisel Z., Smith K., Warren S., Heger A., et al., 2010, ApJS, 189, 240. doi:10.1088/0067-0049/189/1/240

Ferguson J. W., Alexander D. R., Allard F., Barman T., Bodnarik J. G., Hauschildt P. H., Heffner-Wong A., et al., 2005, ApJ, 623, 585. doi:10.1086/428642

Grevesse N., Noels A., 1993, oee..conf, 15

Henyey L., Vardya M. S., Bodenheimer P., 1965, ApJ, 142, 841. doi:10.1086/148357

Huber, D., Bedding, T. R., Stello, D., et al., 2011, Testing Scaling Relations for Solar-like Oscillations from the Main Sequence to Red Giants Using Kepler Data, ApJ, 743, 143p.

Iglesias C. A., Rogers F. J., 1993, ApJ, 412, 752. doi:10.1086/172958

Iglesias C. A., Rogers F. J., 1996, ApJ, 464, 943. doi:10.1086/177381

Jermyn A. S., Bauer E. B., Schwab J., Farmer R., Ball W. H., Bellinger E. P., Dotter A., et al., 2023, ApJS, 265, 15. doi:10.3847/1538-4365/acae8d

Kayhan C., Yıldız M., Çelik Orhan Z., 2019, MNRAS, 490, 1509. doi:10.1093/mnras/stz2634

Kjeldsen H., Bedding T. R., 1995, A&A, 293, 87. doi:10.48550/arXiv.astro-ph/9403015

Kjeldsen H., Bedding T. R., Christensen-Dalsgaard J., 2008, ApJL, 683, L175. doi:10.1086/591667

Kunz R., Fey M., Jaeger M., Mayer A., Hammer J. W., Staudt G., Harissopulos S., et al., 2002, ApJ, 567, 643. doi:10.1086/338384

Marques J. P., Monteiro M. J. P. F. G., Fernandes J. M., 2008, Ap&SS, 316, 173. doi:10.1007/s10509-008-9786-7

Monteiro M. J. P. F. G., 2008, Ap&SS, 316, 121. doi:10.1007/s10509-008-9802-y

Morel P., 1997, A&AS, 124, 597. doi:10.1051/aas:1997209

Morel P., Lebreton Y., 2008, Ap&SS, 316, 61. doi:10.1007/s10509-007-9663-9

Paxton B., Bildsten L., Dotter A., Herwig F., Lesaffre P., Timmes F., 2011, ApJS, 192, 3. doi:10.1088/0067-0049/192/1/3

Paxton B., Cantiello M., Arras P., Bildsten L., Brown E. F., Dotter A., Mankovich C., et al., 2013, ApJS, 208, 4. doi:10.1088/0067-0049/208/1/4

Paxton B., Marchant P., Schwab J., Bauer E. B., Bildsten L., Cantiello M., Dessart L., et al., 2015, ApJS, 220, 15. doi:10.1088/0067-0049/220/1/15

Paxton B., Schwab J., Bauer E. B., Bildsten L., Blinnikov S., Duffell P., Farmer R., et al., 2018, ApJS, 234, 34. doi:10.3847/1538-4365/aaa5a8

Paxton B., Smolec R., Schwab J., Gautschy A., Bildsten L., Cantiello M., Dotter A., et al., 2019, ApJS, 243, 10. doi:10.3847/1538-4365/ab2241

Ricker G. R., Winn J. N., Vanderspek R., Latham D. W., Bakos G. Á., Bean J. L., Berta-Thompson Z. K., et al., 2015, JATIS, 1, 014003. doi:10.1117/1.JATIS.1.1.014003

Rogers F. J., Swenson F. J., Iglesias C. A., 1996, ApJ, 456, 902. doi:10.1086/176705

Stix M., 1989, sun..book, 192

Yıldız M., Çelik Orhan Z., Aksoy Ç., Ok S., 2014, MNRAS, 441, 2148. doi:10.1093/mnras/stu662

Yıldız M., Çelik Orhan Z., Kayhan C., 2016, MNRAS, 462, 1577. doi:10.1093/mnras/stw1709

Yıldız M., Çelik Orhan Z., Kayhan C., 2019, MNRAS, 489, 1753. doi:10.1093/mnras/stz2223

APPENDIX A: SOME EXTRA MATERIAL

If you want to present additional material which would interrupt the flow of the main paper, it can be placed in an Appendix which appears after the list of references.

This paper has been typeset from a TEX/LATEX file prepared by the author.